SUPPLEMENTARY INFORMATION

Hydrogen bonding networks of Nalidixic acid-Copper(II) complexes

Catarina Bravo[a], Filipa Galego[a], Vânia André[a*]

[a] Centro de Química Estrutural, Instituto Superior Técnico, Universidade de Lisboa, Av. Rovisco Pais, 1, 1040-001 Lisboa, Portugal

[*] vaniandre@tecnico.ulisboa.pt

EXPERIMENTAL DETAILS

Synthesis

All reagents were purchased from Sigma and used without further purification.

SYNTHESIS OF $[Cu(NALD)_2]\cdot H_2O$ - **Complex I**

Complex **I** was synthesized by manually grinding together nalidixic acid (0.2 mmol) and $Cu(CH_3COO)_2\bullet H_2O$ (0.1 mmol), with 100 µL of ammonia and 50 µL of water, for 8 minutes. Single crystals were obtained from recrystallization of the compound in a methanol and ammonia solution left to crystallize by slow evaporation of the solvent at room temperature.

FT-IR [KBr, cm^{-1}]: 3643-3416 (ν_{O-H}, water), 3072–2931 (ν_{C-H}, phenyl rings), 1633 ($\nu_{C=O}$), 1579–1409 ($\nu_{C=N}$, $\nu_{C=C}$, phenyl rings), 1321-1261 (ν_{C-N}), 763-755 (δ_{C-H}, phenyl rings).

SYNTHESIS OF $[Cu(NALD)(Phen)(H_2O)][CH_3COO]\cdot 3H_2O$ - **Complex II**

Complex **II** was synthesized by manually grinding together 2 times nalidixic acid (0.2 mmol), 1,10-phenanthroline (0.2 mmol) and $Cu(CH_3COO)_2\bullet H_2O$ (0.2 mmol), with 100 µL of ammonia, for 5 minutes each. Single crystals were obtained from recrystallization of the compound in a DMF and ammonia solution left to crystallize by slow evaporation of the solvent at room temperature.

FT-IR [KBr, cm^{-1}]: 3434-3247 (ν_{O-H}, water), 3083–2940 (ν_{C-H}, phenyl rings), 1629-1608 ($\nu_{C=O}$), 1581–1403 ($\nu_{C=N}$, $\nu_{C=C}$, phenyl rings), 1342-1265 (ν_{C-N}), 898-777 (δ_{C-H}, phenyl rings).

SYNTHESIS OF $[Cu(NALD)(Phen)(NO_3)]\bullet H_2O$ - **Complex III**

To a solution of $Cu(NO_3)_2\bullet 3H_2O$ (0.2 mmol) and 1,10-phenanthroline (0.2 mmol), in 6 mL of ethanol and 10 mL of distilled water, it was added a solution of nalidixic acid in 6 mL of distilled

water and 2 mL of ammonia. The mixture was stirred for 2h at room temperature. Single crystals of complex **III** were obtained after 5 days of slow evaporation of the solvents at room temperature.

The synthesis of complex **III** was reproduced using mechanochemistry by manually grinding together nalidixic acid (0.2 mmol), 1,10-phenanthroline (0.2 mmol) and $Cu(NO_3)_2 \bullet 3H_2O$ (0.2 mmol), with 100 µL of ammonia, for 5 minutes. The obtained powder was then recrystallized in DMF and ammonia.

FT-IR [KBr, cm^{-1}]: 3530-3200 (ν_{O-H}, water), 3070-2940 (ν_{C-H}, phenyl rings), 1620-1600 ($\nu_{C=O}$, ν_{N-O}), 1560–1450 ($\nu_{C=N}$, $\nu_{C=C}$, phenyl rings), 1380 (ν_{N-O}), 1320-1260 (ν_{C-N}), 850-777 (δ_{C-H}, phenyl rings).

SYNTHESIS OF $[Cu(NALD)(Phen)(Cl)]\cdot xH_2O$, where x= 1 - **Complex IV** - or x=4 - **Complex V**

A mixture of both complexes **IV** and **V** was obtained by stirring a solution of $CuCl_2 \bullet 2H_2O$ (0.2 mmol), nalidixic acid (0.2mmol) and 1,10-phenanthroline (0.2 mmol), in 7 mL of DMF and 3 mL of ammonia, for 2h at 50 °C. The single crystals of both complexes **IV** and **V** were obtained by slow evaporation of the solvents at room temperature.

It was possible to obtain complex **V** through mechanochemical syntheses by manually grinding together twice nalidixic acid (0.2 mmol), 1,10-phenanthroline (0.2 mmol) and $CuCl_2 \bullet 2H_2O$ (0.2 mmol), with 100 µL of DMF and 50 µL of ammonia, for 5 minutes each.

FT-IR of complex **IV** [KBr, cm^{-1}]: 3490-3438 (ν_{O-H}, water), 3047-2935 (ν_{C-H}, phenyl rings), 1629 ($\nu_{C=O}$), 1558–1442 ($\nu_{C=N}$, $\nu_{C=C}$, phenyl rings), 1340-1253 (ν_{C-N}), 860-773 (δ_{C-H}, phenyl rings).

Single crystal X-ray Diffraction

Crystals of **I–V** suitable for X-ray diffraction study were mounted with Fomblin© in a cryoloop. Data was collected on a BRUKER D8 QUEST diffractometer with graphite-monochromated radiation (Mo Kα, λ=0.7107 Å) at 293 K. The X-ray generator was operated at 50 kV and 30 mA and the X-ray data collection was monitored by APEX3[1] program. All data were corrected for Lorentzian, polarization and absorption effects using SAINT[2] and SADABS[315] programs. SHELXT[4] was used for structure solution and SHELXL-2014/7[4] was used for full matrix least-squares refinement on F^2. These three programs are included in the package of programs WINGX-Version 2014.1[5]. Non-hydrogen atoms were refined anisotropically. A full-matrix least-squares refinement was used for the non-hydrogen atoms with anisotropic thermal parameters. All the hydrogen atoms bonded to carbon atoms were inserted in idealized positions and allowed to refine in the parent carbon atom. Hydrogen atoms in the water molecules were located from

the electron density map. Table III summarizes data collection and refinement details. Crystallographic data of complexes **I** to **V** were deposited at the Cambridge Crystallographic Data Centre (CCDC 1938699-1938703). Single crystals of **IV** and **V** were of very low quality and weakly diffracting, and therefore, despite several data collections were attempted with different crystals, no good values of Rint were possible to obtain.

MERCURY 4.1.3[6] was used for packing diagrams and PLATON[7] for details on the hydrogen bond interactions.

Crystal data and details of data collection for **I–V** are reported in Table I, and hydrogen bond details are given in Table II.

*Table I. Crystal Data and Structure Refinement Details for complexes **I–V**.*

	I	II	III	IV	V
Formula	$[C_{24}H_{22}Cu_1N_4O_6]\cdot 2(H_2O)$	$[C_{12}H_{11}Cu_1N_2O_3\cdot C_{12}H_8N_2\cdot H_2O]^{+}\cdot CH_3COO^{-}\cdot 3H_2O$	$[C_{12}H_{11}Cu_1N_2O_3\cdot C_{12}H_8N_2\cdot NO_3]\cdot H_2O$	$[C_{12}H_{11}Cu_1N_2O_3\cdot C_{12}H_8N_2\cdot Cl]\cdot H_2O$	$[C_{12}H_{11}Cu_1N_2O_3\cdot C_{12}H_8N_2\cdot Cl]\cdot 4H_2O$
Fw	562.02	606.08	555.00	528.45	582.50
Crystal Form, colour	Plate, blue	Block, blue	Needle, blue	Block, blue	Plate, blue
Crystal size (mm)	0.02 x 0.14 x 0.24	0.10 x 0.10 x 0.10	0.010 x 0.12 x 0.27	0.10 x 0.16 x 0.22	0.08 x 0.05 x 0.03
Crystal system	Monoclinic	Triclinic	Triclinic	Monoclinic	Triclinic
space group	$P2_1/c$	P-1	P-1	$P2_1/n$	P-1
a, Å	8.2633(5)	9.4804(11)	7.9957(9)	8.998(3)	9.069(6)
b, Å	7.4357(4)	10.7188(11)	12.0271(11)	19.758(5)	12.511(10)
c, Å	19.1577(12)	14.0027(15)	12.6970(14)	12.654(4)	12.708(9)
α, deg	90.00	72.559(5)	94.074(5)	90.00	116.23(6)
β, deg	99.821(2)	82.036(6)	97.486(6)	98.021(9)	91.24(6)
γ, deg	90.00	78.107(6)	108.309(5)	90.00	97.94(6)
Z	2	2	2	4	2
V, Å^3	1159.86(12)	1323.9(3)	1141.2(2)	2227.6(11)	1275.4(17)
T, K	293(2)	293(2)	293(2)	293(2)	293(2)
D_c, g cm^{-3}	1.609	1.520	1.615	1.576	1.517
μ(Mo Kα), mm^{-1}	1.002	0.887	1.016	1.141	1.013
θ range (°)	2.501 – 27.492	2.168 – 25.000	2.277 – 24.998	2.508 – 24.997	2.682 – 24.999
refl. collected	17756	34137	35549	28999	33096
independent refl.	2663	4663	4025	3841	4491
R_{int}	0.0759	0.1889	0.1155	0.2160	0.2823
R_1 [a], wR_2 [b] [$I \geq 2\sigma(I)$]	0.0484, 0.1114	0.0626, 0.1458	0.0497, 0.1168	0.0685, 0.1543	0.0799, 0.1897
GOF on F^2	1.074	1.038	1.040	1.020	1.024

[a] $R_1 = \Sigma||F_o| - |F_c||/\Sigma|F_o|$. [b] $wR_2 = [\Sigma[w(F_o^2 - F_c^2)^2]/\Sigma[w(F_o^2)^2]]^{1/2}$

*Table II – Hydrogen bonding details for complexes **I-V***

	Sym. Op.	D–H···A	*d* (D–H) (Å)	*d* (H···A) (Å)	*d* (D···A) (Å)	D$\hat{H}$A (°)
I	2-x, -1/2+y, 3/2-z	O_{1w}–H_{3w}···O_3	0.91(5)	2.49(5)	3.189(5)	133(5)
	x, y, z	O_{1w}–H_{4w}···O_3	0.93(3)	2.00(3)	2.861(5)	154(3)
II	1-x, -y, 1-z	O_{1w}–H_{1w}···O_3	0.90(6)	1.94(7)	2.796(6)	159(8)
	x, y, z	O_{1w}–H_{2w}···O_5	0.91(2)	1.78(3)	2.672(6)	166(8)
	-x, -y, 2-z	O_{2w}–H_{3w}···O_4	0.88(4)	1.95(6)	2.790(8)	159(7)
	x, y, z	O_{2w}–H_{4w}···O_4	0.89(6)	1.92(6)	2.785(8)	163(6)
	x, y, z	O_{3w}–H_{5w}···O_{1w}	0.90(4)	2.01(6)	2.886(8)	164(8)
	-1+x, y, z	O_{3w}–H_{6w}···O_3	0.88(7)	2.14(8)	2.994(7)	164(7)
	x, y, z	O_{4w}–H_{7w}···O_{2w}	0.88(5)	2.14(6)	2.931(8)	149(6)
	x, y, z	O_{4w}–H_{8w}···O_5	0.90(7)	1.87(7)	2.770(8)	175(9)
III	x, y, z	O_{1w}–H_{1w}···O_3	0.90(6)	1.99(6)	2.877(7)	169(7)
	1+x, y, z	O_{1w}–H_{2w}···O_5	0.90(5)	2.03(6)	2.907(8)	164(8)
IV	-1/2+x, 3/2-y, -1/2+z	O_{1w}–H_{1w}···Cl_1	0.89(7)	2.46(7)	3.297(7)	156(8)
	x, y, z	O_{1w}–H_{2w}···O_3	0.89(7)	2.10(7)	2.985(9)	174(9)
V	x, y, z	O_{1w}–H_{1w}···O_3	0.86	2.04	2.728(10)	136
	2-x, 1-y, -z	O_{1w}–H_{2w}···$Cl_{.1}$	0.86	2.41	3.173(8)	148
	x, y, z	O_{2w}–H_{3w}···O_3	0.85	1.97	2.762(12)	154
	x, y, z	O_{2w}–H_{4w}···O_{4w}	0.90(11)	2.03(10)	2.711(12)	132(12)
	x, y, z	O_{3w}–H_{5w}···O_{2w}	0.90(13)	1.86(12)	2.707(14)	157(11)
	1-x, 1-y, -z	O_{3w}–H_{6w}···Cl_1	0.90(9)	2.41(11)	3.307(11)	174(12)
	2-x, 2-y, 1-z	O_{4w}–H_{7w}···O_{1w}	0.86	1.93	2.772(13)	167
	1-x, 2-y, 1-z	O_{4w}–H_{8w}···O_{3w}	0.87	2.00	2.780(13)	148

Powder X-ray Diffraction

Patterns were collected on a D8 Advance Bruker AXS diffractometer with a Linxeye-XE detector, and copper radiation source (Cu Kα, λ=1.5406 Å), operated at 40 kV and 30 mA. The program MERCURY 4.1.3[6] was used to obtain the diffraction patterns calculated from single-crystal data. The purity of the bulk was always verified by comparing the calculated and observed powder X--ray diffraction patterns.

Infrared Spectroscopy

Spectra were recorded on a Nexus-Thermo Nicolet spectrometer (64 scans and resolution of 4 cm^{-1}) in the 4000-400 cm^{-1} range. Samples were diluted in KBr (1:100 in weight).

Differential Scanning Calorimetry and Thermogravimetry

Combined measurements were carried out on a SETARAM TG-DTA 92 thermobalance under nitrogen flow with a heating rate of 10 $^{o}C \cdot min^{-1}$. The samples' mass was in the range 5-10 mg.

Hot-stage microscopy

Hot-stage experiments were carried out using a Linkam TP94 device connected to a Linkam LTS350 platinum plate. Images were collected with the imaging software Cell, from an Olympus SZX10 stereomicroscope.

Stability tests at different temperatures

Powder stability experiments were carried out using a Binder oven, heating the samples for a period of 24h at 50 ^{o}C and at 80 ^{o}C. The PXRD patterns were the measured with the regular parameters.

CRYSTAL STRUCTURES

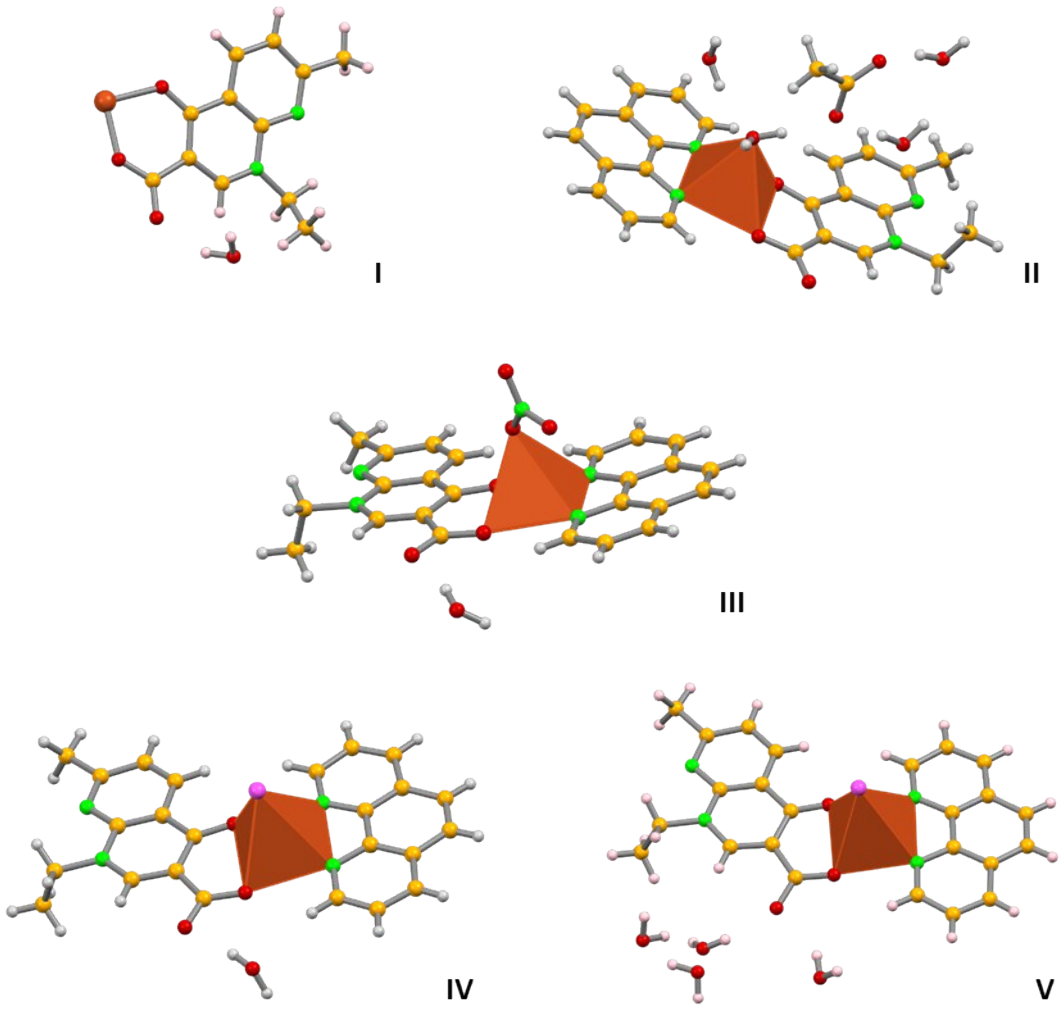

*Figure 1 – Asymmetric units of complexes **I** to **V***

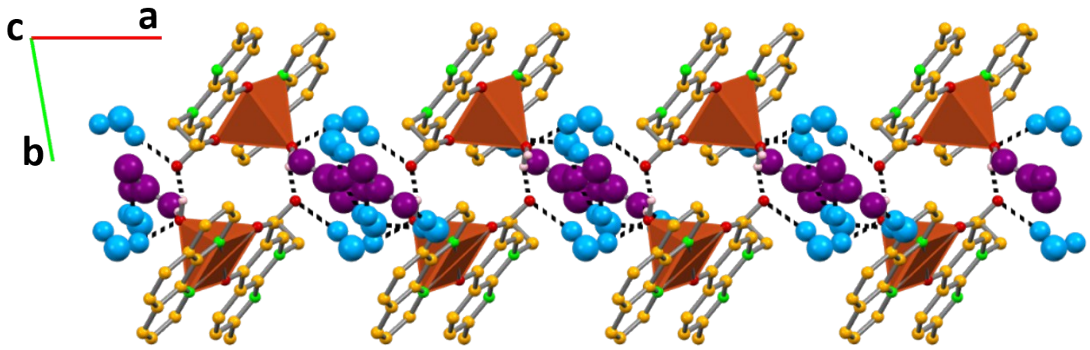

*Figure 2 – Supramolecular arrangement of **II** in a view along the c axis. Water molecules are represented in blue and the acetate anions in purple, both using spacefill representation; hydrogen atoms of nalidixic acid and 1,10-phenanthroline were omitted for clarity*

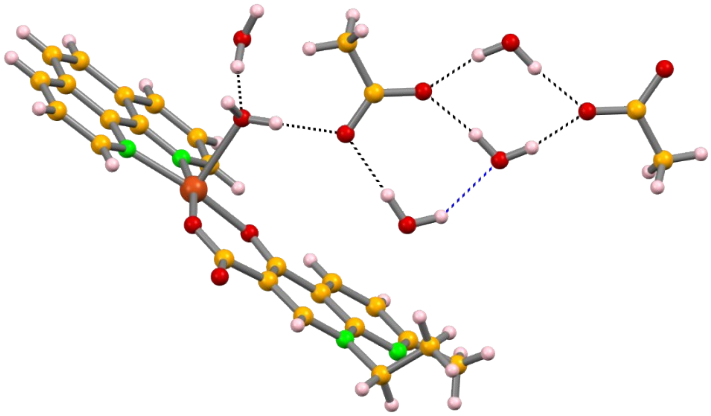

*Figure 3 – Depiction of the water clusters discrete chain D2 (represented in blue dashed line) in complex **II***

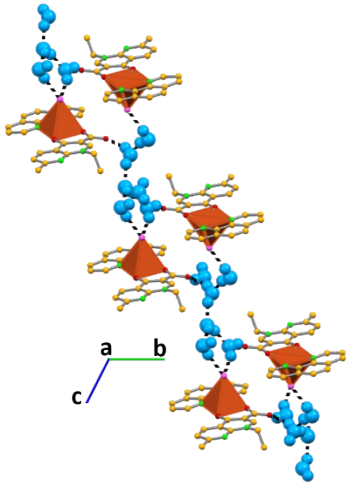

*Figure 4 - Supramolecular arrangement of **V** in a view along the a axis. Water molecules are represented in blue, using spacefill representation; hydrogen atoms of nalidixic acid and 1,10-phenanthroline were omitted for clarity*

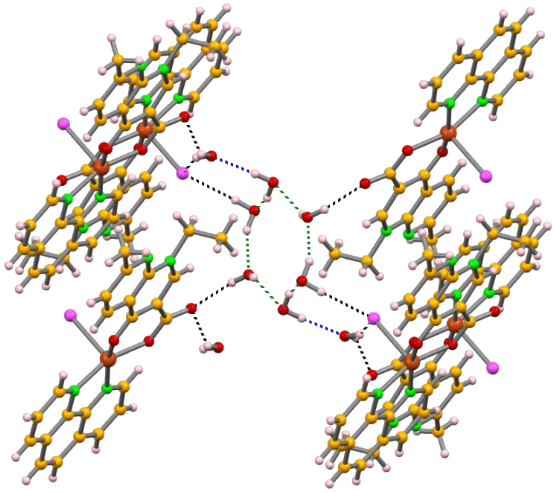

*Figure 5 - Depiction of the water clusters discrete chains D2 (represented in blue dashed lines) and R6 rings (represented by the green dashed lines) in complex **V***

PURITY OF THE SAMPLES

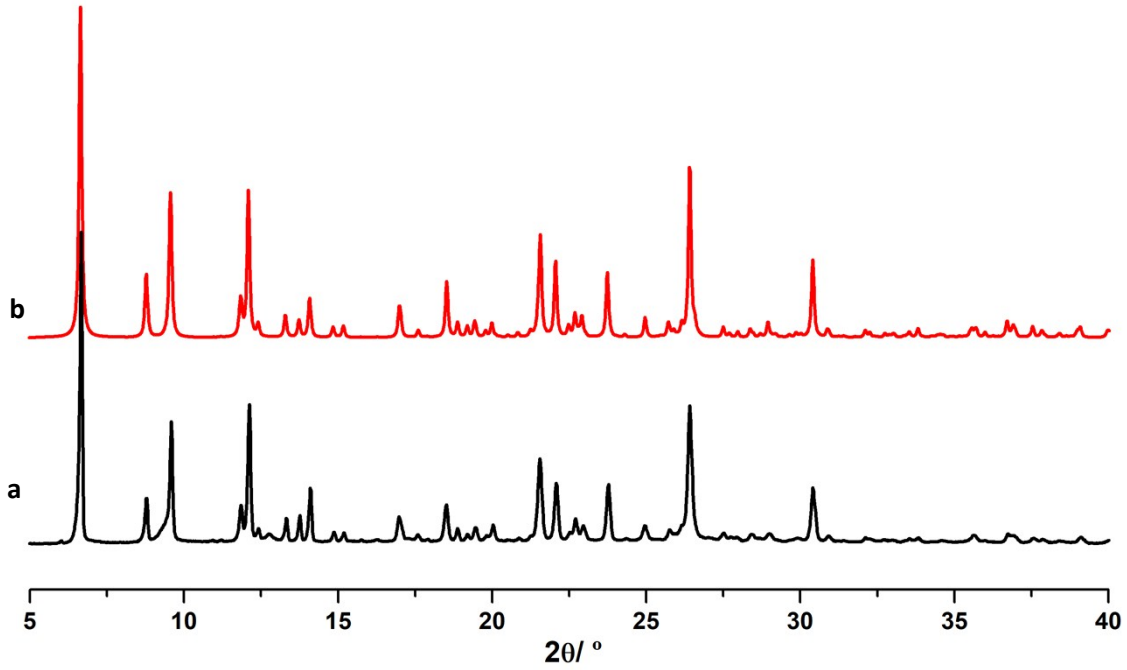

*Figure 7. PXRD patterns of (a) complex [Cu(NALD)(Phen)(H_2O)][CH_3COO]•3H_2O (**II**) and (b) simulated from the crystal of complex [Cu(NALD)(Phen)(H_2O)][CH_3COO]•3H_2O (**II**)*

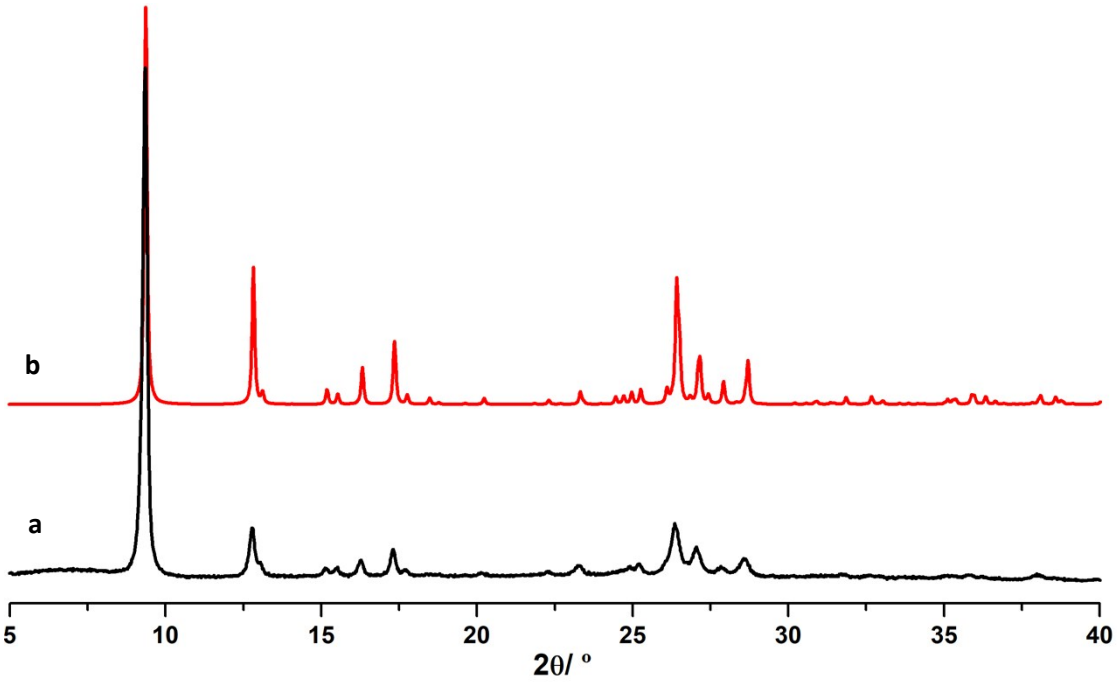

*Figure 6. PXRD patterns of (a) complex [$Cu(NALD)_2$]•H_2O (**I**) and (b) simulated from the crystal of complex [$Cu(NALD)_2$]•H_2O (**I**)*

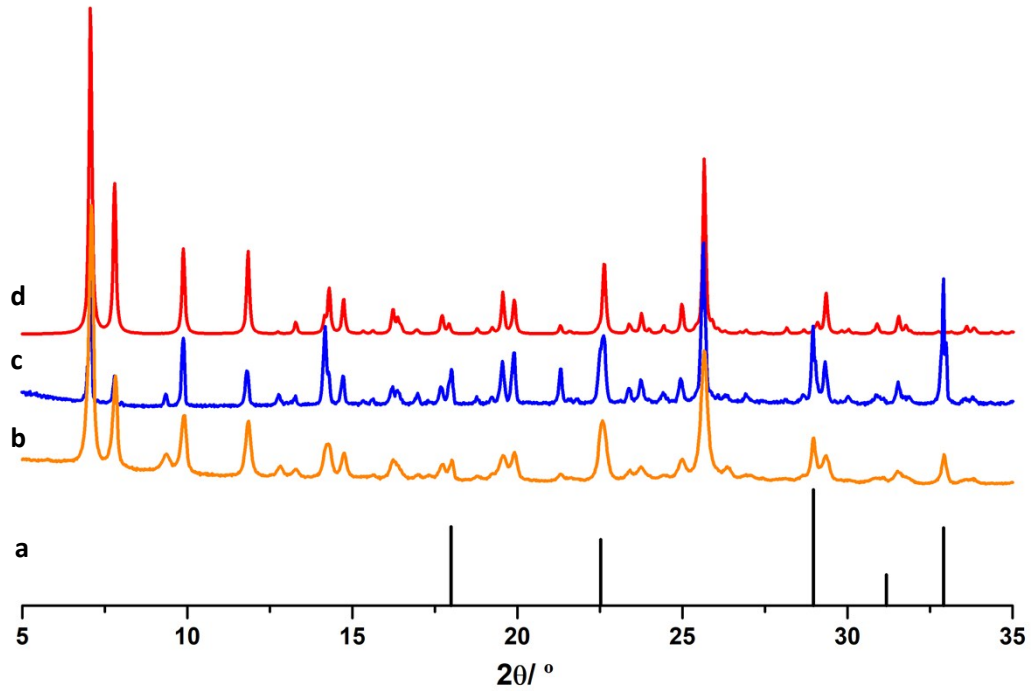

*Figure 8. XRPD patterns of (a) $NH_4 NO_3$ salt obtained from the database, (b) mechanochemical synthesis of complex [Cu(NALD)(Phen)(NO_3)]•H_2O (**III**), (c) crystals obtained by solution synthesis, (d) simulated from the crystal of the complex [Cu(NALD)(Phen)(NO_3)]•H_2O (**III**)*

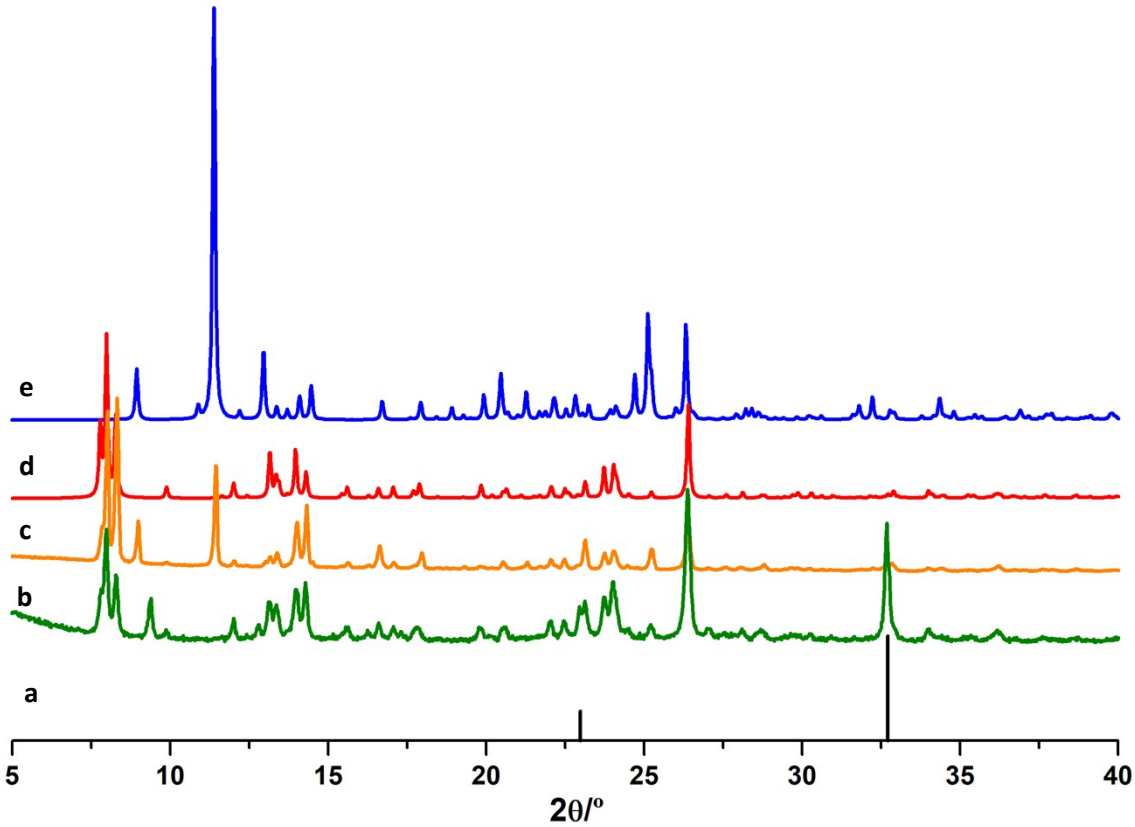

*Figure 9. XRPD patterns of (a) NH_4Cl salt obtained from the database, (b) mechanochemical synthesis of complex [Cu(NALD)(Phen)(Cl)]•$4H_2O$ (**V**), (c) mixture of both complexes obtained by solution synthesis, (d) simulated from the crystal [Cu(NALD)(Phen)(Cl)]•$4H_2O$ (**V**), (e) simulated from the crystal [Cu(NALD)(Phen)(Cl)]•H_2O (**IV**)*

INFRARED SPECTROSCOPY DATA

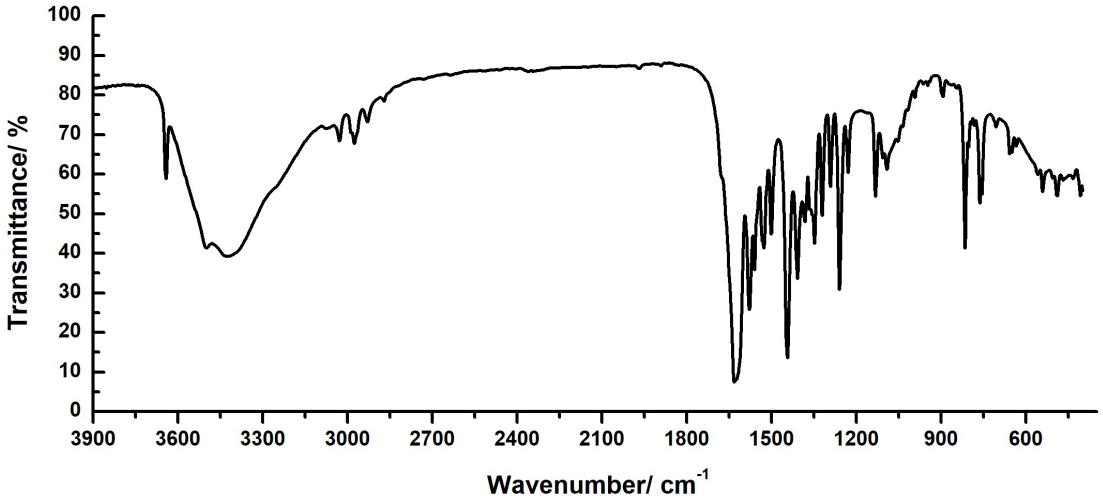

*Figure 10. Fourier-transform infrared (FTIR) spectrum of the complex [Cu(NALD)$_2$] •H_2O (**I**) in KBr Pellets*

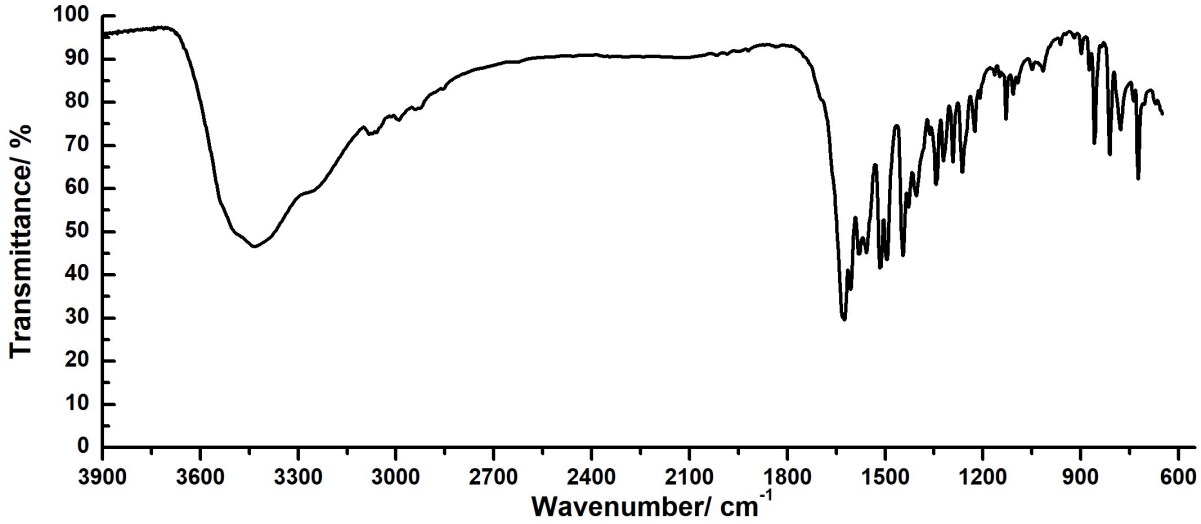

*Figure 11. Fourier-transform infrared (FTIR) spectrum of the complex [Cu(NALD)(Phen)(H_2O)][CH_3COO]•3H_2O (**II**) in KBr Pellets*

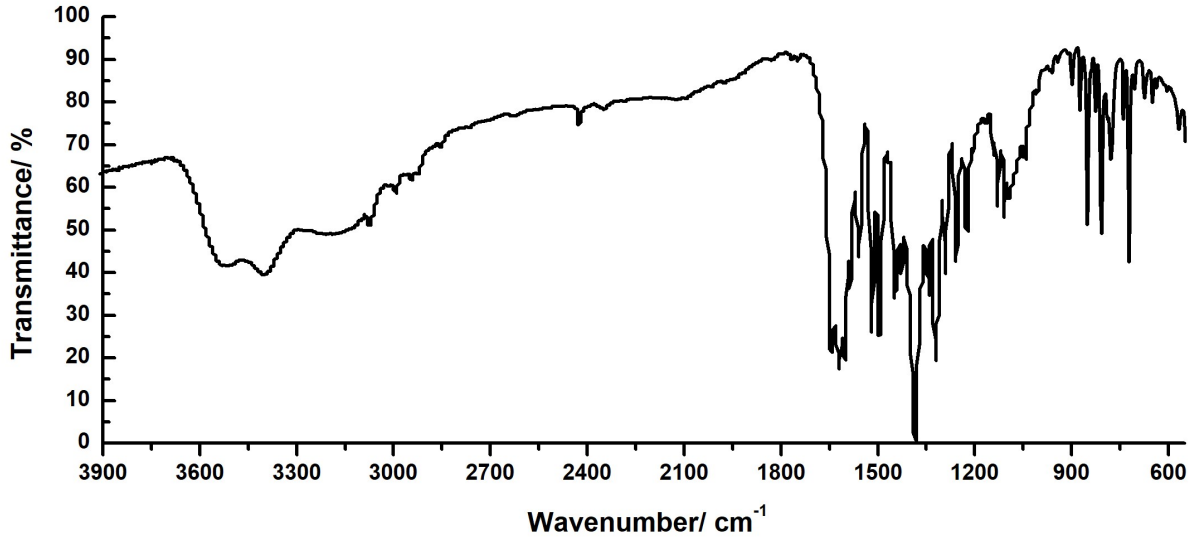

*Figure 12. Fourier-transform infrared (FTIR) spectrum of the complex [Cu(NALD)(Phen)(NO_3)]•H_2O (**III**) in KBr Pellets*

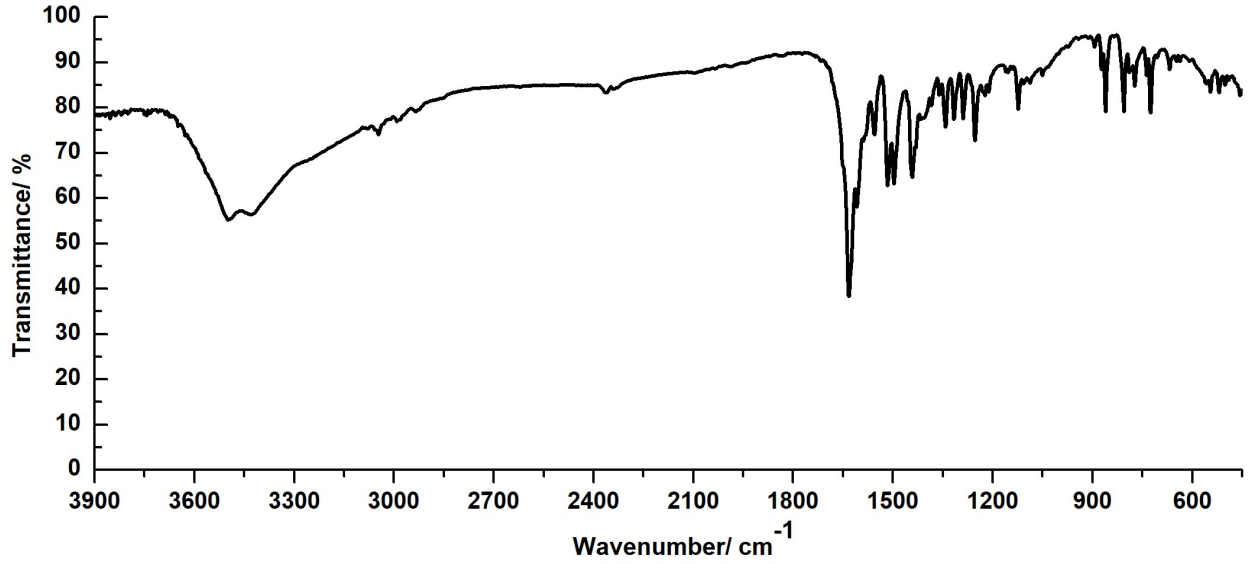

*Figure 13. Fourier-transform infrared (FTIR) spectrum of the complex [Cu(NALD)(Phen)(Cl)]•H_2O (**IV**) in KBr Pellets*

THERMAL STABILITY ASSESSMENT

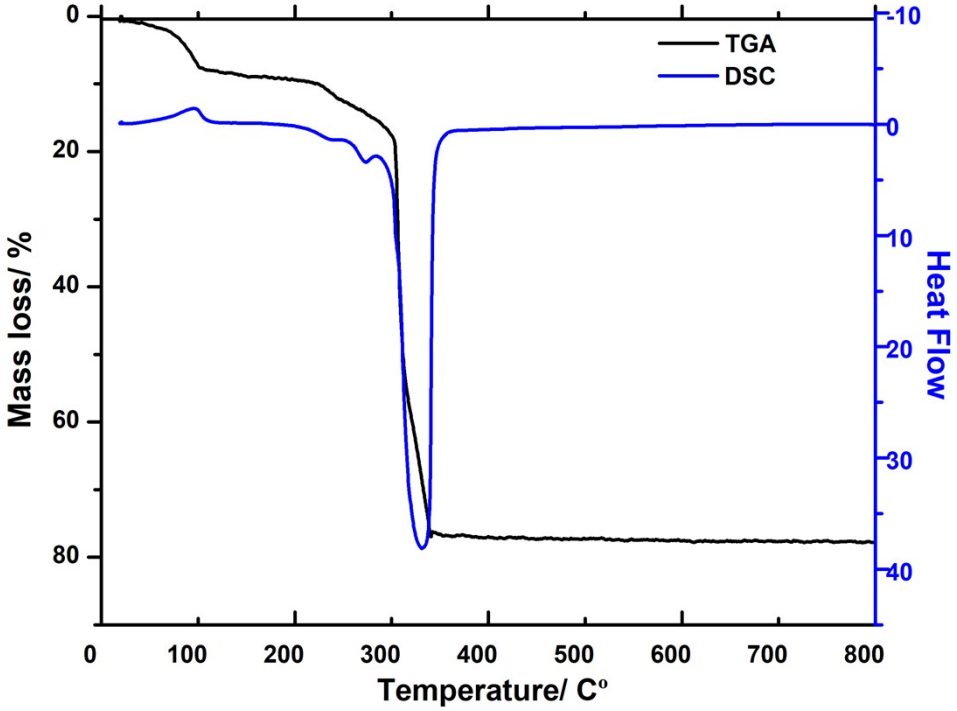

*Figure 14. DSC and TGA for complex $[Cu(NALD)_2]•H_2O$ (**I**)*

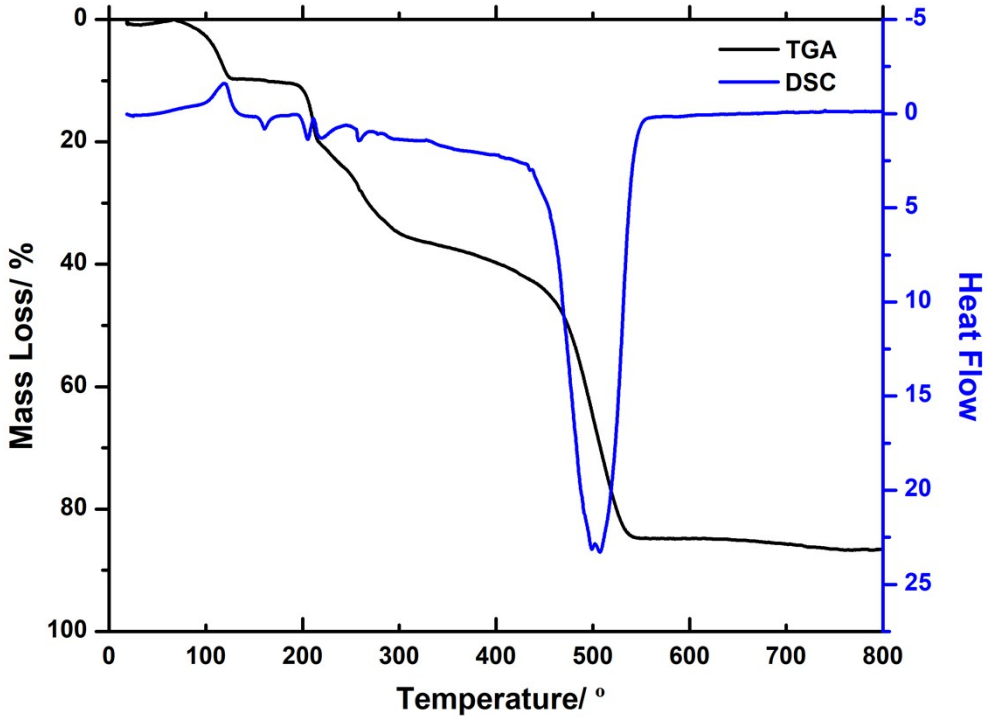

*Figure 15. DSC and TGA for complex $[Cu(NALD)(Phen)(H_2O)][CH_3COO]•3H_2O$ (**II**)*

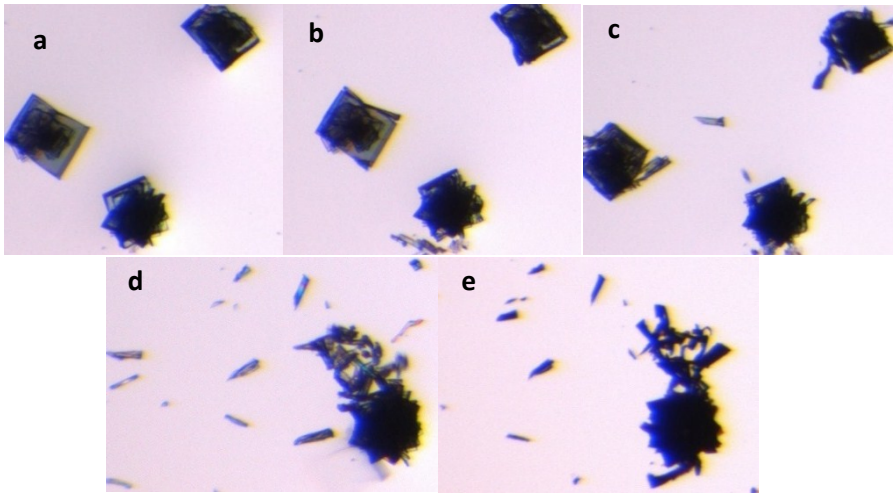

*Figure 16. HSM of complex $[Cu(NALD)_2]•H_2O$ (**I**) at (a) 29.0 °C, (b) 84.0 °C, (c) 106.7 °C, (d) 156.9 °C and (e) 345.0 °C*

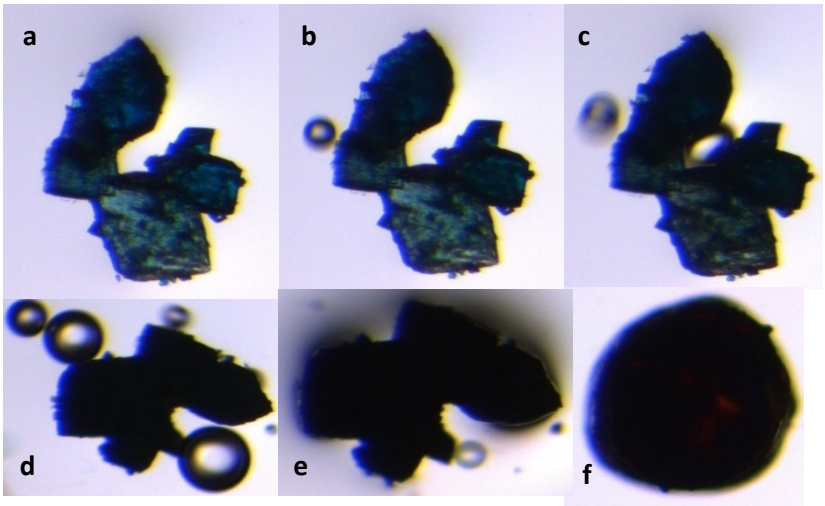

*Figure 17. HSM of complex $[Cu(NALD)(Phen)(H_2O)][CH_3COO]•3H_2O$ (**II**) at (a) 26.6 °C, (b) 105.5 °C, (c) 108.8 °C, (d) 124.7 °C, (e) 203.3 °C and (f) 211.1 °C*

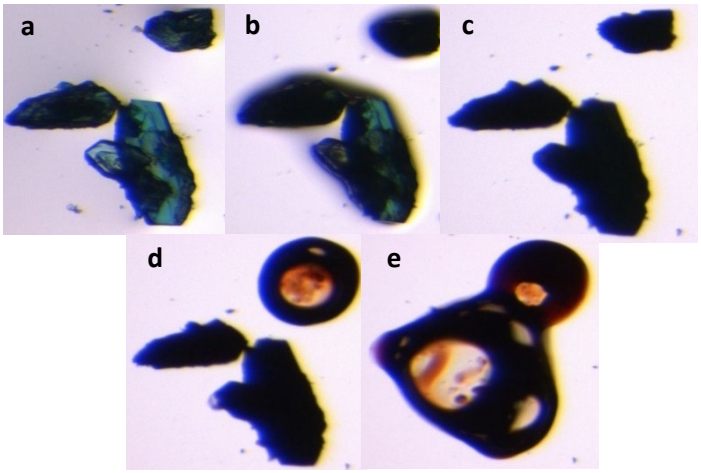

*Figure 19. HSM of complex [Cu(NALD)(Phen)(Cl)]•H_2O (**IV**) at (a) 30.0 ^oC, (b) 168.9 ^oC, (c) 200.0 ^oC, (d) 276.2 ^oC and (e) 276.5 ^oC.*

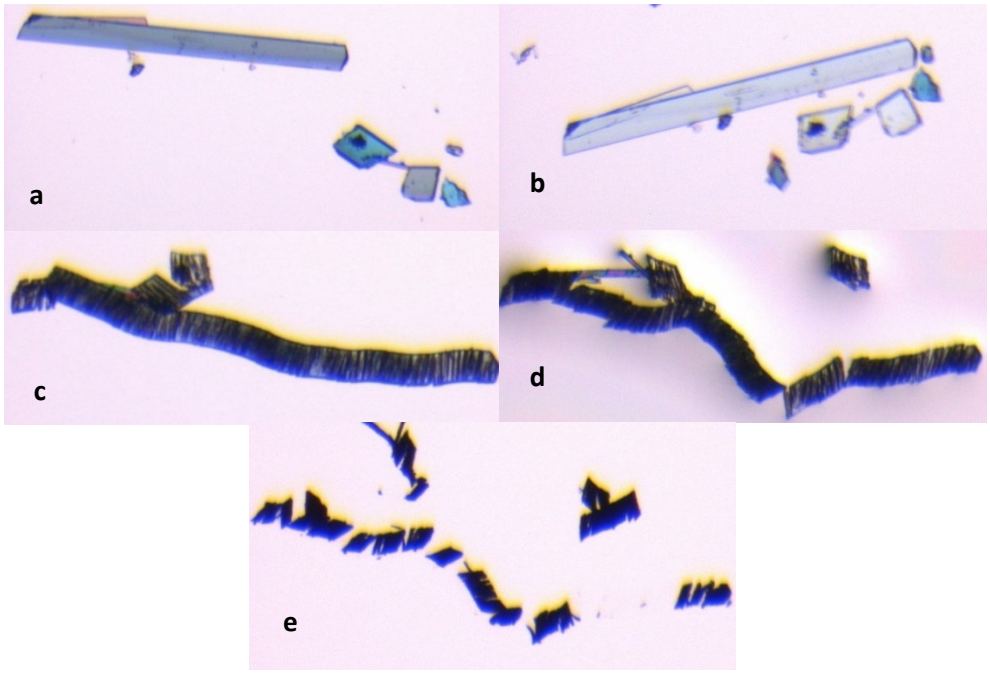

*Figure 18. HSM of complex [Cu(NALD)(Phen)(NO_3)]•H_2O (**III**) at (a) 30.0 ^oC, (b) 59.2 ^oC, (c) 120.8 ^oC, (d) 182.1 ^oC and (e) 350.0 ^oC.*

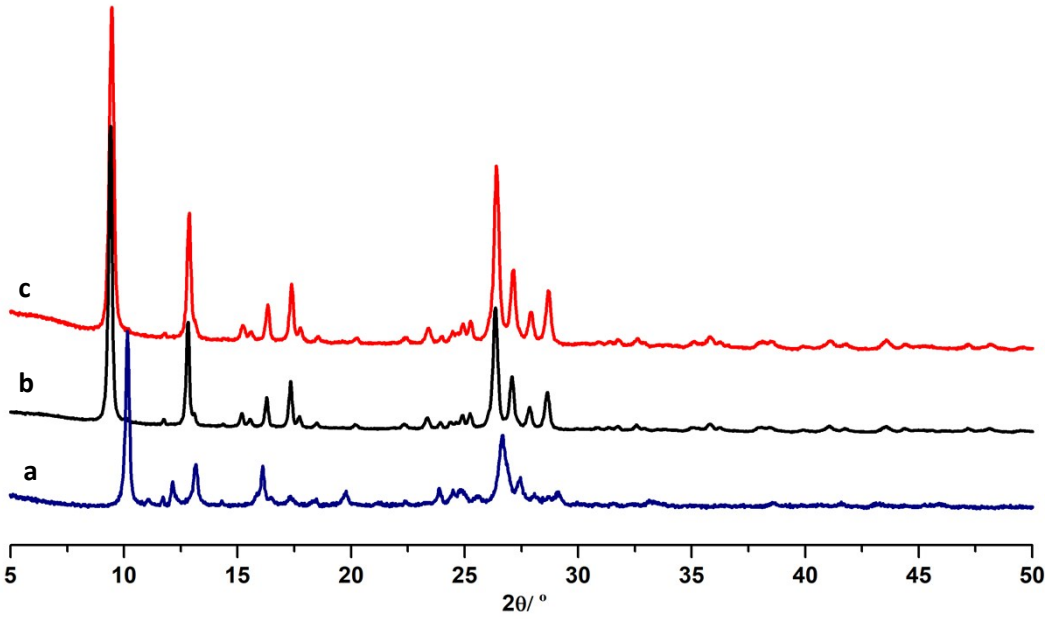

*Figure 20. PXRD patterns of the complex $[Cu(NALD)_2]•H_2O$ (**I**) measured after staying 24h at different temperatures: at 80 °C (a), at 50 °C (b) and at room temperature (c)*

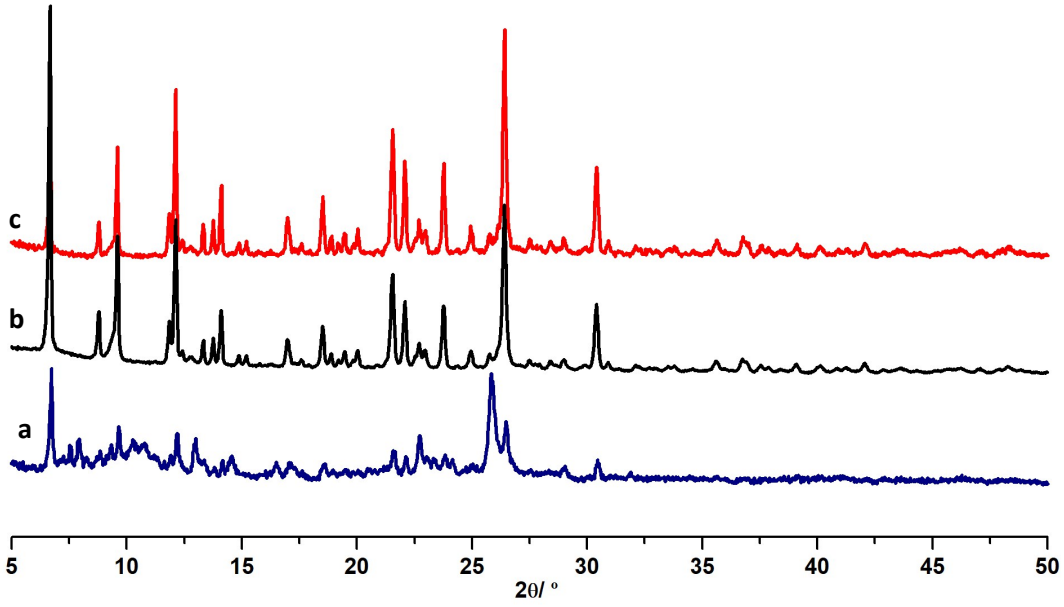

*Figure 21. PXRD patterns of the complex $[Cu(NALD)(Phen)(H_2O)][CH_3COO]•3H_2O$ (**II**) measured after staying 24h at different temperatures: at 80 °C (a), at 50 °C (b) and at room temperature (c)*

HIRSHFELD SURFACE ANALYSIS

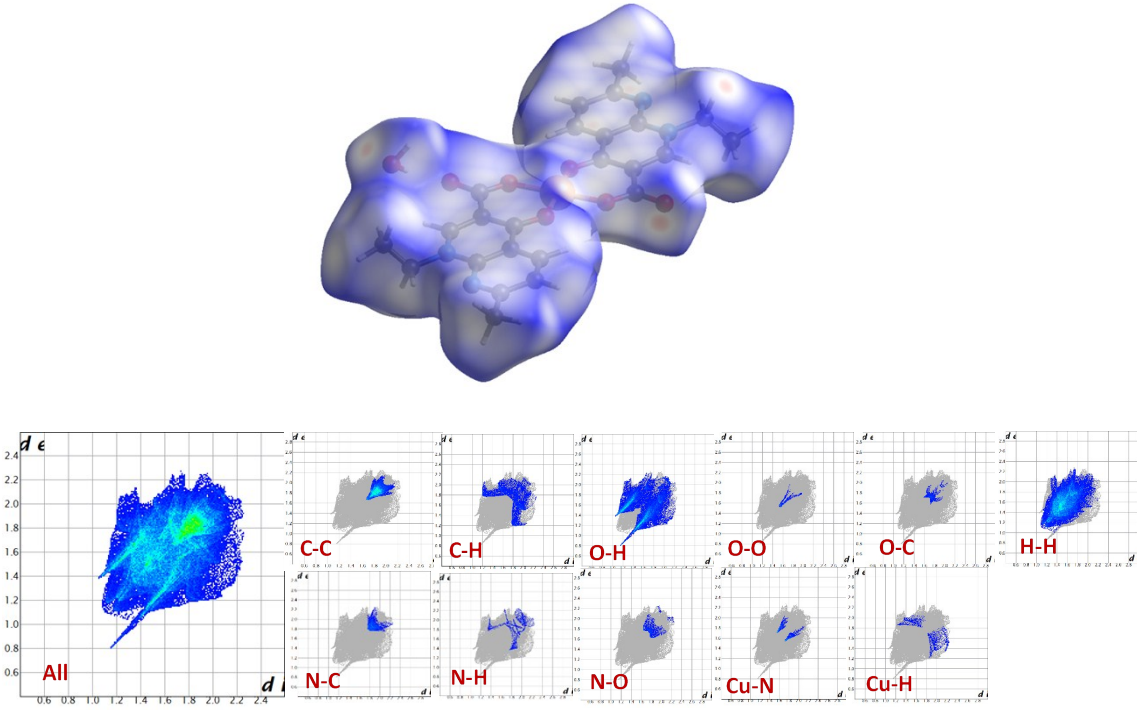

Figure 22. Hirshfeld surface mapped with d_{norm}, with surfaces shown as transparent to allow the visualization of the compound (top) and two-dimensional fingerprint plots (bottom) for complex I

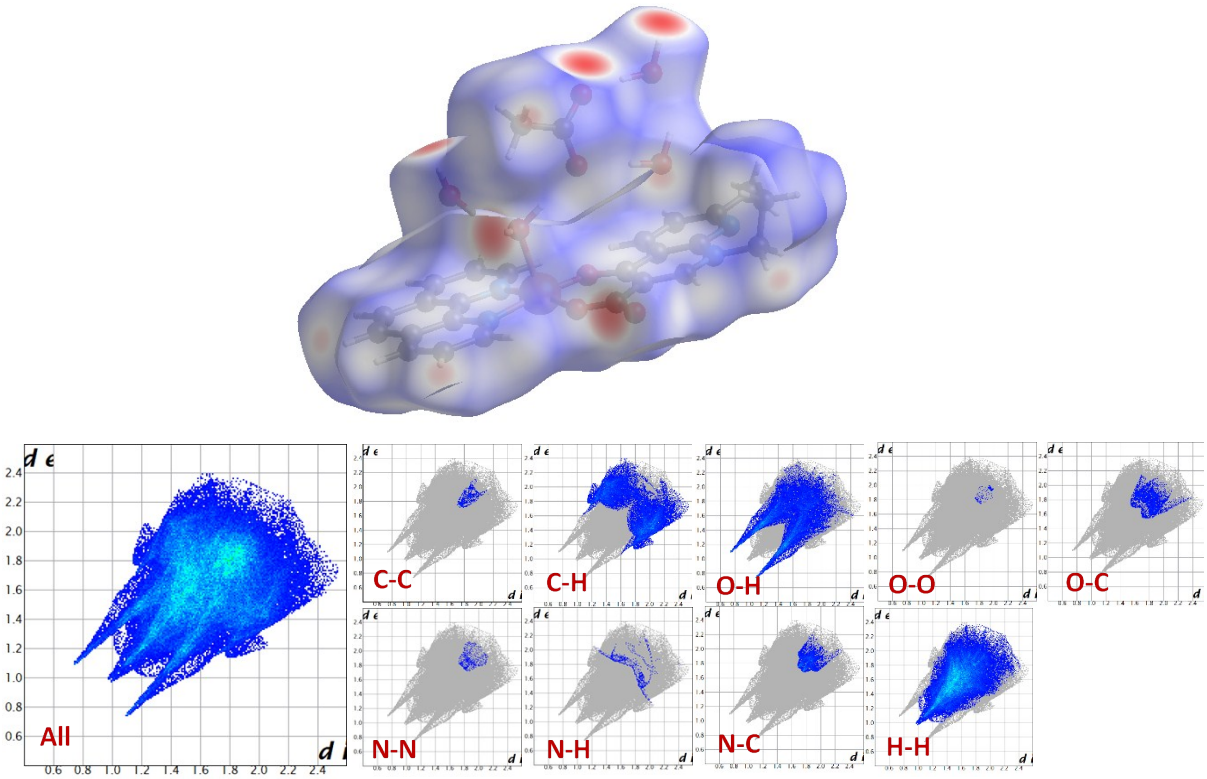

Figure 23. Hirshfeld surface mapped with d_{norm}, with surfaces shown as transparent to allow the visualization of the compound (top) and two-dimensional fingerprint plots (bottom) for complex II

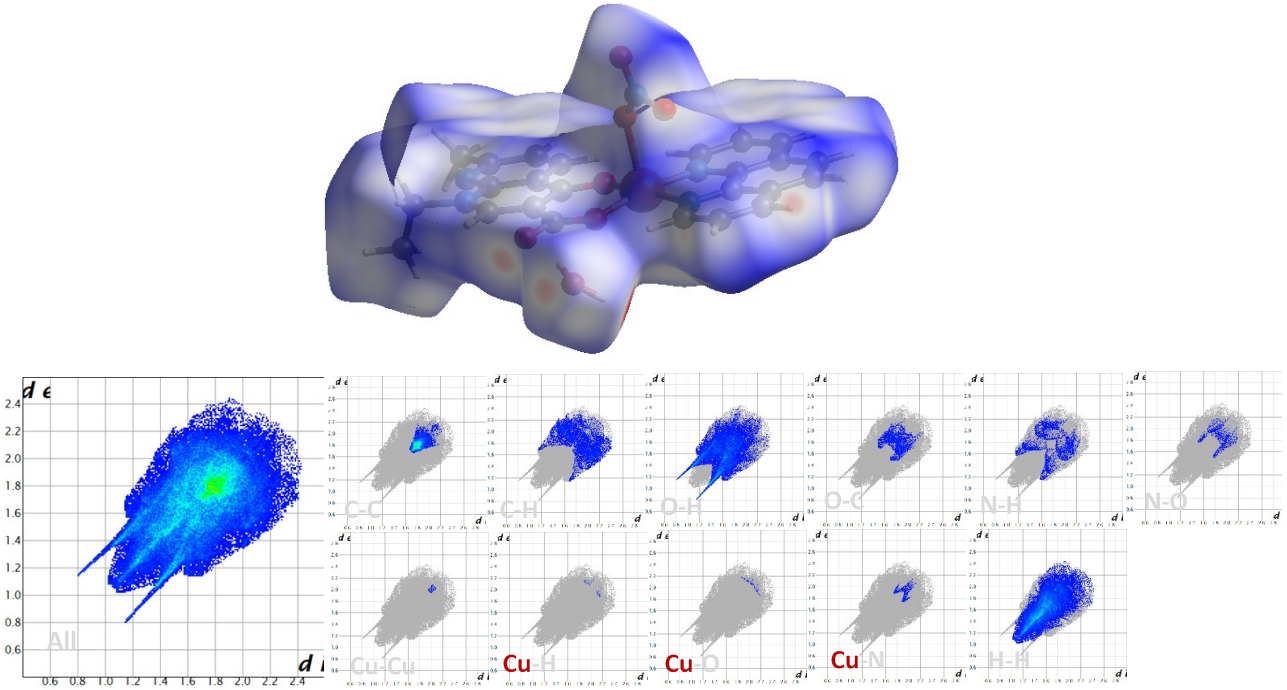

Figure 24. Hirshfeld surface mapped with d_{norm}, with surfaces shown as transparent to allow the visualization of the compound (top) and two-dimensional fingerprint plots (bottom) for complex III

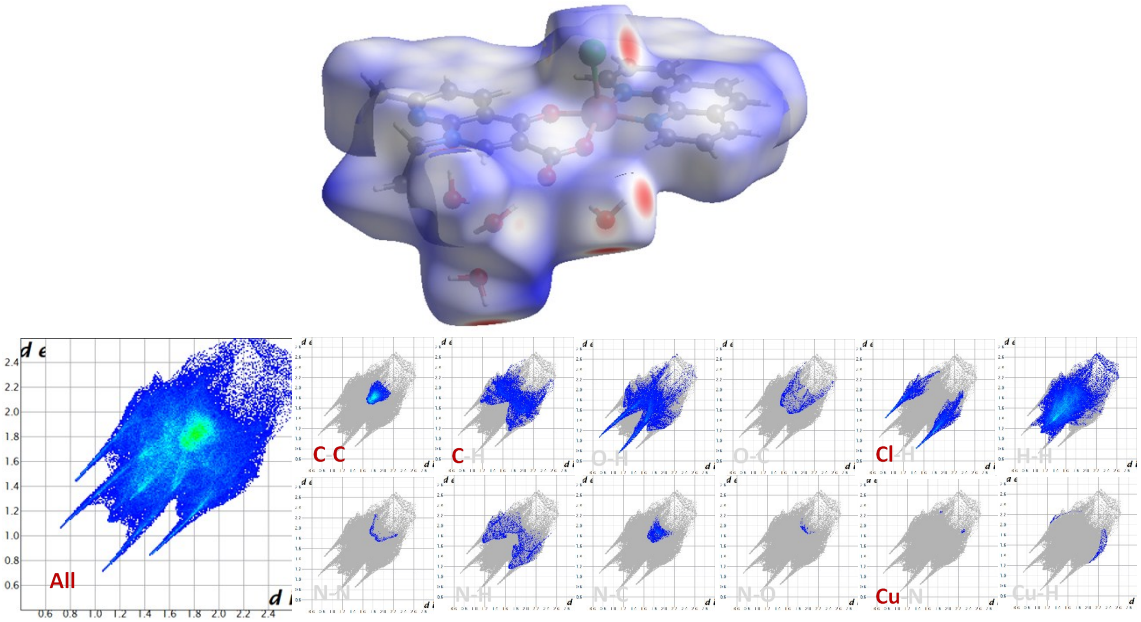

Figure 25. Hirshfeld surface mapped with d_{norm}, with surfaces shown as transparent to allow the visualization of the compound (top) and two-dimensional fingerprint plots (bottom) for complex IV

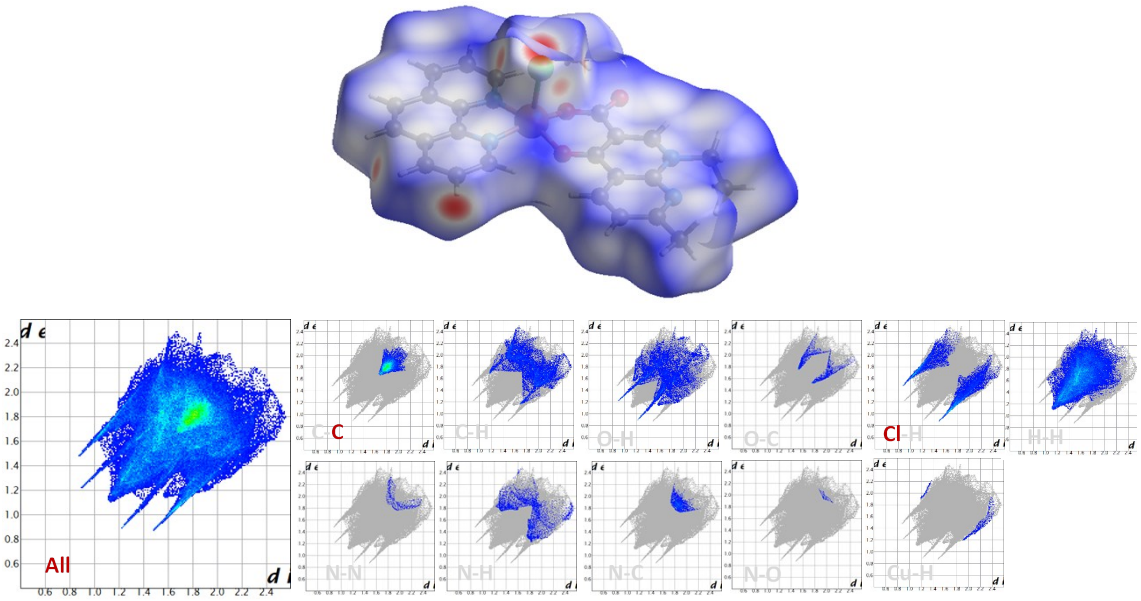

Figure 26. Hirshfeld surface mapped with d_{norm}, with surfaces shown as transparent to allow the visualization of the compound (top) and two-dimensional fingerprint plots (bottom) for complex V

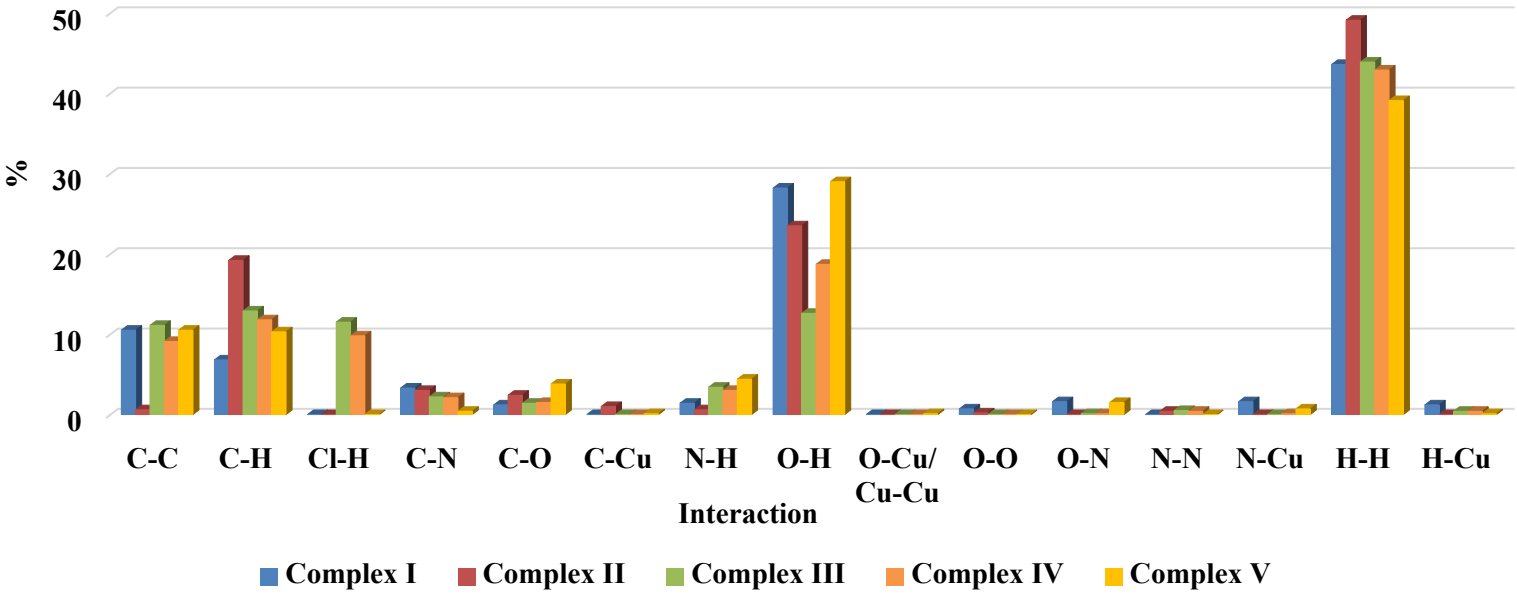

Figure 27. Graphical comparison of Hirshfeld surface analysis' percentages of interactions for complexes I to V.

REFERENCES

1. Bruker-AXS *APEX3*, Ver. 2017.3-0; Bruker AXS: Madison, Wisconsin, USA, 2014..
2. Bruker-AXS *SAINT*,*Bruker Analytical Systems: Madison,WI*, 2014.
3. Bruker-AXS *SADABS,Bruker Analytical Systems: Madison,WI*, 2014.
4. G. M. Sheldrick, *Acta Crystallographica Section C*, 2015, **C71**, 3-8.
5. L. J. Farrugia, *J. Appl. Cryst.*, 1999, **32**, 837-838.
6. C. F. Macrae, I. J. Bruno, J. A. Chisholm, P. R. Edgington, P. McCabe, E. Pidcock, L. Rodriguez-Monge, R. Taylor, J. van de Streek and P. A. Wood, *Journal of Applied Crystallography*, 2008, **41**, 466-470.
7. A. L. Spek, *Acta Crystallographica Section D-Biological Crystallography*, 2009, **65**, 148-155.